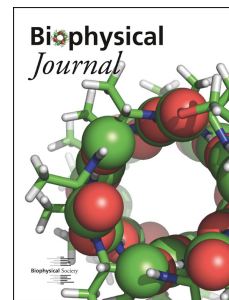


# Journal Pre-proof

Conductance of porous media depends on external electric fields

Leonid P. Savtchenko, Kaiyu Zheng, Dmitri A. Rusakov



PII: S0006-3495(21)00149-1

DOI: <https://doi.org/10.1016/j.bpj.2021.02.012>

Reference: BPJ 11003

To appear in: *Biophysical Journal*

Received Date: 1 April 2020

Accepted Date: 1 February 2021

Please cite this article as: Savtchenko LP, Zheng K, Rusakov DA, Conductance of porous media depends on external electric fields, *Biophysical Journal* (2021), doi: <https://doi.org/10.1016/j.bpj.2021.02.012>.

This is a PDF file of an article that has undergone enhancements after acceptance, such as the addition of a cover page and metadata, and formatting for readability, but it is not yet the definitive version of record. This version will undergo additional copyediting, typesetting and review before it is published in its final form, but we are providing this version to give early visibility of the article. Please note that, during the production process, errors may be discovered which could affect the content, and all legal disclaimers that apply to the journal pertain.

© 2021 Biophysical Society.

# Conductance of porous media depends on external electric fields

Leonid P. Savtchenko, Kaiyu Zheng, Dmitri A. Rusakov

UCL Queen Square Institute of Neurology, University College London, London, UK

## Abstract

In obstacle-filled media, such as extracellular or intracellular lumen of brain tissue, effective ion diffusion permeability is a key determinant of electrogenic reactions. Although this diffusion permeability is thought to depend entirely on structural features of the medium, such as porosity and tortuosity, brain tissue shows prominent non-ohmic properties, the origins of which remain poorly understood. Here, we explore Monte Carlo simulations of ion diffusion in a space filled with overlapping spheres, to predict that diffusion permeability of such media decreases with stronger external electric fields. This dependence increases with lower medium porosity while decreasing with radial (2D or 3D) compared to homogenous (1D) fields. We test our predictions empirically in an electrolyte chamber filled with microscopic glass spheres and find good correspondence with our predictions. A theoretical insight relates this phenomenon to a disproportionately increased dwell time of diffusing ions at potential barriers (or traps) representing geometric obstacles, when the field strength increases. The dependence of medium ion-diffusion permeability on electric field could be important for understanding conductivity properties of porous materials, in particular for the accurate interpretation of electric activity recordings in brain tissue.

*Keywords:* porous media, electrodiffusion, brain electricity

Correspondence: [d.rusakov@ucl.ac.uk](mailto:d.rusakov@ucl.ac.uk) or [leonid.savtchenko@ucl.ac.uk](mailto:leonid.savtchenko@ucl.ac.uk)

**SIGNIFICANCE STATEMENT**

From nanomaterials to animal tissues, diffusion permeability of porous media has been attributed entirely to their structure, which is often summarised as porosity and tortuosity. Here we simulate a sphere-filled space to find that its conductance decreases with stronger electric fields, and confirmed this in a physical experiment, with a theoretical treatment highlighting its key parameters. This finding has some potentially fundamental implications for our understanding of electricity in porous media. For instance, it suggests that routinely recorded brain field potentials may not necessarily scale linearly with the strength of current sources inside the brain tissue. On the microscopic scale, it predicts retarded diffusion of charged molecules, heterogeneous charge accumulation, and possibly supra-linear heat dissipation with increased electrical activity.

## INTRODUCTION

Physiological signalling in animal tissue relies on rapid diffusion of electrolyte ions in the extracellular (or intracellular) space filled with relatively immobile obstacles, from macromolecules to microscopic cellular structures. Compared to a free medium, diffusion in obstacle-filled, or porous, media is retarded. According to the classical Nernst–Einstein equation, electrolyte conductivity  $G$  scales with ion diffusivity so that

$$G = \frac{F^2}{RT} \sum_{n=1}^i D_n q_n^2 C_n \quad (1)$$

where  $q_n$ ,  $C_n$ , and  $D_n$  are respectively, the valence, concentration, and diffusivity of the  $n$ th ion species,  $F$  is Faraday's constant,  $R$  is gas constant, and  $T$  is absolute temperature (Table 1). Thus, at constant ion concentrations,  $G$  is proportional to diffusivity (which may not be the case when ion concentrations vary or are spatially non-uniform). Generally, retardation of ion diffusion by obstacles corresponds to increased electrical resistance, which in turn affects the scale and dynamics of electric events critical for cell function, particularly in the brain, both on the scale of tissue (1) and the nanoscale (2). Numerous studies have focused on the brain extracellular space to establish that its net diffusion retardation effect is determined by the medium porosity  $\alpha$  (space volume fraction available for diffusion) and tortuosity  $\lambda$ , which corresponds to the apparent diffusion coefficient  $D_{app} = D_{free} / \lambda^2$  ( $D_{free}$  is free-medium diffusivity) (1, 3), or otherwise diffusion permeability  $\theta = D_{app} / D_{free} = \lambda^{-2}$  (4). The values of  $\alpha$ ,  $\lambda$ , or  $\theta$  in brain tissue have been evaluated on the scale of several microns and above (3, 5, 6). Recently, advances in live super-resolution imaging has extended this quest to the nanoscale (7, 8), whereas molecular mobility in the extracellular and intracellular lumen on the nanoscale has been evaluated using time-resolved anisotropy-FLIM (9). In this context, it has routinely been assumed that the architectural features of porous media (such as  $\lambda$ ,  $\theta$ ,  $\alpha$ , or more complex shape variables) principally define their effective conductivity (10, 11).

When electric field is present, ion movement follows the classical Nernst-Planck relationship

$$\frac{dC}{dt} = -\nabla \cdot (J_D + J_E) \quad (2)$$

where  $C$  is ion concentration,  $J_D = -D\nabla C$  and  $J_E = -Dq \frac{F}{RT} C \nabla V$  are, respectively, diffusion and electric drift (migration) components,  $V$  is field potential (gradient  $\nabla V$  is equivalent to field strength  $E$ ). Eqs. 1-2 are key to the traditional interpretation of electrophysiological recordings: it assumes constant electrolyte conductivity  $G$  which depends simply on the bulk concentration of ions. Indeed, in the case of the mammalian brain, the common assumption has been that the Nernst-Planck formalism of electrodiffusion applies to the tortuous extracellular space with diffusivity corrected for  $\theta$  (12-14).

More recently, however, it has been shown that brain tissue shows prominent non-ohmic properties that might affect interpretation of local field potentials (15-18) whereas physical tests in porous ceramics indicated that permittivity of such media could depend on the electric field strength (19). There has been a significant progress in advancing theoretical work that focuses on electrodiffusion in porous media (e.g., discussed in (20, 21), including brain tissue (22). On the nanoscale, anomalous diffusion arising due to diffusion obstacles and electric field interactions in cell membranes and neuronal dendrites has also been explored (23, 24). However, the influence of external electric fields on ion diffusion permeability of such obstacle-filled media remains poorly understood.

Here, we focus on this particular issue as a first principle, without attempting to address or generalise evaluation of apparent diffusivity or permittivity for porous media of various types. To understand the basic phenomenon, we therefore explore Monte Carlo (MC) simulations mimicking electrodiffusion of charged particles across the space filled, to a varied degree, with inert, partly overlapped spherical obstacles. While not critical for establishing theoretical principles, our simulation parameters were chosen to roughly replicate the movement of small ions, on the microscopic scale, in the interstitial (or intracellular) brain tissue lumen filled with macromolecules and other nanoscopic obstacles. Our simulations predict that increasing the external field strength lowers porous medium diffusion permeability, thus deviating from the classical Nernst-Planck theory. We test this prediction by using voltammetry measurements in electrolyte filled with non-polarizing dielectric (glass), microscopic spheres, and suggest a first-approximation theoretical insight into the underlying principles.

## MATERIALS AND METHODS

### Monte Carlo simulations: Electrodiffusion

MC simulation algorithms were designed and run using MATLAB, based on the classical Nernst-Planck relationship (Equation 2), as detailed and tested against experimental recordings earlier (25, 26). The standard random walk procedure for individual particles (ions) was thus implemented, in which the electric field drift (migration) was calculated from the particle

speed as  $\frac{d\mathbf{r}}{dt} = -\mu\mathbf{E}$  where mobility  $\mu = Dq\frac{F}{RT}$ , vector  $\mathbf{E} = \nabla V$  is the field strength, and  $\mathbf{r}$

is the coordinate vector ( $r$  is radial co-ordinate). Thus, ion particles positioned at time  $t$  at point  $\mathbf{r}(x, y, z)$  were moved to point  $\mathbf{r}_1(x_1, y_1, z_1)$  over time increment  $\Delta t$  so that, in the case

of 1D field,  $x_1 = x + \Delta x * \delta + \Delta t \frac{eED}{kT} \frac{x}{r}$ , with  $E = 0$  for particle displacement into  $y$  and  $z$

directions,  $\Delta x$  corresponds to the mean square displacement in the Einstein's diffusion equation for 1D Brownian motion  $\Delta x^2 = 2D\Delta t$ ,  $\delta$  denotes a 'delta-correlated' (independently seeded, uncorrelated) uniform random number from the  $(-1, 1)$  range to reflect that Brownian particles are equally likely to move into either direction,  $e$  is elementary charge, and  $k$  is the Boltzmann constant (Table 1). In the case of the 2D radial field (inside a flat and narrow 2D slab), this expression had  $E = 0$  for  $z$  direction; in the 3D radial field (3D open space), all directions had the field term. As the drift component was added at every diffusion step, the diffusion coefficient calculation was dealing with time and distance in a fixed co-ordinate system.

To avoid occasional numerical deadlocks for particles trapped near the space dead-ends formed by aggregated overlapped spheres (Fig. S1B), we implemented the duty-cycle translational movements in a contiguous 3D space, over all directions, rather than over the rectangular 3D-lattice vertices used by us and many others previously. The duty cycle time step  $\Delta t$  (usually  $< 0.1 \mu\text{s}$ ) was set to be small enough to prevent particles from 'tunnelling' through the smallest, 6 nm wide obstacles.

The basic 'reference value' field strength  $E_0$  was set at  $10^4$  V/m, which roughly corresponds to the field generated by a synaptic current of 10-50 pA towards the centre of the 10-15 nm thick, 0.5  $\mu\text{m}$  wide synaptic cleft, with the medium resistance of  $\sim 100$  Ohm cm (9, 27, 28). Accordingly, for stronger electric fields ( $E > 2E_0$ ) we adopted  $\Delta t < 0.01 \mu\text{s}$ . For the sake of

simplicity, and to separate the effect of field geometry per se, we have assumed constant field strength  $E$  for both uniform (1D) and radial (2D and 3D) fields whereas under the common 2D and 3D scenarios, field is attenuated with a factor of  $r^{-1}$  and  $r^{-2}$ , respectively where  $r$  is the distance to the infinitesimal central source. Instead of incorporating these factors in our calculations, we considered the 1D case as the first-principles scenario, and addressed the effect of weakening the field separately, by exploring  $E$  values over an order of magnitude.

The particle-wall interaction was simulated as an elastic collision, and electrostatic interactions with the obstacle surfaces were ignored, on the assumption that the dimensions of the free diffusion space were much larger than the electrolyte double-layer.

The initial conditions routinely included 2000 particles injected instantaneously in the arena centre (within a 10 nm sphere at the coordinate origin, outside any obstacle). This reflected the case when ions flowing through the open channel generate the field in which they and other ions diffuse, such as inside the synaptic cleft (28). We also ran arena-size trials for each new condition using 200 diffusing particles (see below). Ten full trials with 2000 particles each were carried out for the statistical estimates of average diffusion permeability values, with the sphere distributions generated anew every trial. In addition, we systematically ran single control trials involving 2000 particles, to verify the computational stability for the diffusion steps, sphere distributions, and the interactions between particles and obstacles.

### **Monte Carlo simulations: Sphere-filled space**

The main parameter controlling the distribution of spheres is the volume fraction  $\beta$  occupied by them. The  $\beta$  value was calculated by (a) scattering  $10^5$  test points uniformly randomly across the entire space, and (b) calculating the proportion of the point falling outside the spheres. We verified that increasing the number of such test points to  $10^6$  altered  $\beta$  by  $<1\%$ , suggesting asymptotic accuracy. The space (arena) dimensions were set large enough to reach a stationary value for the apparent diffusion coefficient under the strongest electrical field (fluctuation was less than  $\pm 1\%$  for the last 20% of the simulated diffusion time). As noted above, the arena size was routinely trialled and established using ad hoc simulations with 200 particles, under the strongest tested electric field, without spheres.

To fill the space with overlapping spheres that have a distributed size, the following algorithm was adopted. First, we prohibited spheres to occupy a 3 nm wide space around the co-ordinate origin where the particles start their random walk. Second, in each duty cycle, we generated a random sphere location (set of co-ordinates) with the arena space, and the random radius value (distributed in accord with the designated density function) for the sphere. Third, we repeated the cycle until  $\beta$  approaches the required value with ~5% accuracy.

To replicate our empirical arrangement with glass spheres, we attempted an algorithm filling the space with equally sized non-overlapping spheres. Random packing of equal spheres has a theoretical density maximum of ~64%, assuming that the arena size is much larger than that of spheres (29). In computational practice, however, as the volume fraction  $\beta$  occupied by the simulated spheres reaches ~50%, it becomes progressively difficult to insert further spheres. In the majority of cases, the algorithm stalls due to the lack of available space. It turns out that a similar deadlock occurs when the spheres have a pre-defined distribution of their size, at least in the case of even distribution. Therefore, we asked whether the cases of overlapping versus non-overlapping spheres differ significantly in terms of the apparent diffusion coefficient, and found little difference, at least for  $\beta < 0.5$  (see Fig. S1D). This was consistent with the observation that the overlaps occupied only a small fraction (<4% for  $\beta = 0.5$ ) of the arena volume, thus suggesting little effect overall, which also applies to enhanced trapping due to the electric field.

The overall size (cut-off distance) of the diffusion arena was determined by the condition that it should be large enough to contain >99% particles during at least 0.5 ms post-release in the strongest-field case  $E = 5E_0$  and with  $\beta = 0$  (free space, no obstacles). At the same time, the arena had to be sufficiently small to allow technically feasible computation times, which increased supra-linearly with greater  $\beta$  or with the number of spheres introduced as obstacles.

### **Computing environment**

Simulations were carried out on a dedicated, ad hoc-built 8-node BEOWULF-style diskless PC cluster running under the Gentoo LINUX operating system (kernel 4.12.12), an upgraded version of the cluster described earlier (5). Individual nodes comprised an HP ProLiant DL120 G6 Server containing a quad-core Intel Xeon X3430 processor and 8GB of DDR3 RAM. Nodes were connected through a NetGear Gigabit Ethernet switch to a master

computer that distributes programs and collects the results on its hard disk. Optimization and parallelization routines were implemented by AMC Bridge LLC (Waltham, MA).

### Calculating the apparent diffusion coefficient

The apparent diffusion coefficient for the particle cohort, averaged over time  $t$ , in any of the three directions, was calculated as  $D_x = \frac{1}{2N} \sum_{i=1}^N (x_i^2 / t)$  (similar for  $y$  and  $z$ ) where  $N$  is the number of diffusing particles, and  $x_i^2$  reports the particle's mean square displacement over time  $t$ . The diffusion coefficient values were calculated continuously during simulation runs, as long as all original diffusing particles remained within the simulation arena. Normally, once a single particle has left the open boundary of the simulation area, computations stopped.

### Analytical solutions of the Nernst Planck electrodiffusion equations

In analytical estimates of the particle concentration profiles, we solved the Nernst-Planck equation using the built-in MATLAB function *pdepe*. This function enables solving initial-boundary value problems for the parabolic-elliptic type of partial differential equations.

### Conductance measurements

Electrolyte conductance was measured using a classical shunt resistor method (e.g., p. 175 in (30)). Various voltages supplied by a constant voltage source with maximum current limited to 2A (TTi EX4210R 42V 10A model) were applied to a pre-sterilised, industry-standard electroporation chamber (Molecular BioProducts, MBP #5520; WxLxH: 2 mm x 10 mm x 25 mm; Fig. 4A). Because of large current passing through the circuit at high voltage steps, a shunt resistor of 10 A/V (RS257-391) was connected in series to the chamber, from which a small voltage drop across the resistor was measured using a national instrument analogue to digital converter (NI BNC-2090). To deal with any resistive heating effects in the chamber under high currents, we applied short (10 ms) voltage pulses, with a high current reed relay (Cynergy3 S8-0504) connected in series prior to the chamber. The short 10 ms pulse applied to the circuit had no resistive heating effect: the monitored solution temperature in the chamber was 23-24°C throughout tests. Signal timing was gated by a pulse generator (AMPI Master 8), which was triggered from the same national instrument board using acquisition control software WinWCP (University of Strathclyde).

Three different solutions were made: deionised water (H<sub>2</sub>O, Elgar Purelab machine, resistivity 15 MOhm / cm at 25°C), sodium chloride (NaCl, Sigma S7653, 153 mM solution in deionised water solution), and ACSF. The ACSF solution composition was as follows: NaCl (Sigma S7653) 126mM, KCl (Sigma P9333) 2.5mM, MgSO<sub>4</sub>·7H<sub>2</sub>O (Sigma M1880) 1.3mM, NaH<sub>2</sub>PO<sub>4</sub> (Sigma S0751) 1.25mM, glucose (Sigma G8270) 10mM, NaHCO<sub>3</sub> (Sigma S6014) 26mM, CaCl<sub>2</sub>·2H<sub>2</sub>O (Sigma C3881) 2mM. The electrolyte strength was thus chosen to be in the physiological range, below the levels (>0.2M) at which, classically, ion-ion interactions could affect conductivity (31).

DC Voltages were applied to the opposite electrodes in the chamber (Fig. 4A), and small voltages across the shunt resistor were measured and converted to currents. The procedure was carried out in a free solution and then repeated with 13-45 μm lime soda glass spherical microbeads (MO-SCI Speciality Products 201-002-003). The beads were slowly (to avoid void formations) loaded into a ~150 μL freshly prepared solution until the chamber was full (Fig. 4B). The electrolyte volume required to fill the chamber volume occupied by the spheres provided an estimated value of  $\beta = 30 \pm 2\%$ .

Because electrical conductance depends on the temperature it was also important to avoid temperature rises. This was achieved by using short 10 ms voltage steps, with 60 s resting periods: the solution temperature thus held at 23-24°C. The short electrical pulse also minimises electrode polarisation, which might in principle lead to an accumulation of ionic species near the surface hence unwarranted chemical reactions. Special care was taken to avoid bubble formation and accumulation in the solution during electric pulses: tests were terminated upon detection of any microscopic bubbles (usually after several trials). To avoid such and further time-dependent concomitants of the pulse application, we used only the first 3 ms of the pulse, and no more than five trials per cuvette.

### **Data availability**

The datasets generated during and/or analysed during the current study are available from the corresponding authors upon request.

### **Source code availability**

The datasets source codes used in the current study are available from the corresponding authors.

## RESULTS

### Electrodiffusion in uniform 1D electric field

We first asked to what extent geometric obstacles would affect ion movements along a narrow long cylinder (diameter  $\ll$  length), a basic case of 1D diffusion. We note that, although in this case the overall diffusion flux is 1D, on the scale compatible with cylinder diameter diffusion trajectories and obstacle geometries are essentially 3D. For the sake of simplicity, we set the free-medium diffusion coefficient at  $D_{free} = 1 \mu\text{m}^2/\text{ms}$ , which is typical for small ions in aqueous solutions, and the cylinder diameter at  $0.1 \mu\text{m}$ , to roughly represent extra- or intracellular lumen of brain tissue. Zero-size diffusing particles were released in the cylinder centroid and allowed to move freely (Materials and Methods, Fig. 1A, Fig. S1A), with the cylinder walls providing a reflecting boundary. To mimic macromolecular hindrance, small spheres with an evenly distributed diameter over the 3-33 nm range, were scattered uniformly, with overlap, throughout the space (Materials and Methods). Overlapping spheres could sometimes form dead-ends for diffusing particles (Fig. S1B) reflecting non-convex geometries of real microscopic obstacles. The Monte-Carlo algorithm incorporating Brownian movement and electric field drift (Materials and Methods) stochastically directed the particle flow around obstacles, roughly following the field lines around dielectric spheres (Fig. S1C). Although our simulations adopted a uniform field throughout the space, and thus ignored its distortion near dielectric spheres, the comparison of limiting cases (uniform versus zero-field near spheres) indicated that the related diffusivity error was fairly negligible ( $\sim 6\%$  at the strongest field, Fig. S1D). We have also found that changing the non-overlapping to overlapping sphere pattern altered  $D_{app}$  values only within  $\sim 7\%$  at  $\beta \sim 0.4$ , and within  $\sim 4\%$  at  $\beta \sim 0.3$  (Fig. S1E), thus projecting a smaller still effect at smaller  $\beta$ .

Equipped with these settings, we sought to test four scenarios, for  $\beta$  taking four values between 0-0.5, to reflect diffusion retardation on the nanoscale assessed with time-resolved fluorescence anisotropy imaging (9). The time-averaged apparent diffusion coefficient  $D_{app}$  showed significant variability in the initial stages of the test, reflecting anomalous diffusion (Fig. 1B, zero-field), as discussed previously (32). Reassuringly, in a free medium ( $\beta = 0$ )  $D_{app}$  was converging to  $D_{free}$  (Fig. 1B, black dotted line; Fig. S1B). Simulations also showed

that  $D_{app}$  decreased monotonously with greater  $\beta$  (Fig. 1B), consistent with earlier assessments of macroscopic diffusion in porous brain tissue (4, 33, 34).

We next introduced uniform electric field that was collinear with the cylinder axis (Materials and Methods). To mimic the case of an ion channel current that generates voltage gradient for the current-carrying and other ions in the nearby lumen, we considered the outward field direction that would force particles away from the diffusion source (Fig. 1A, arrows). We explored a range of field strength  $E$  centred around  $E_0 = 10^4$  V/m, which roughly represents the field generated by a synaptic current carried mainly by  $\text{Na}^+$  ions towards the synaptic cleft centre at small excitatory synapses (Materials and Methods). The simulation outcome was somewhat unexpected. Introducing geometric hindrance retarded particle diffusion to a greater degree under electric field if compared with the zero-field scenario in the same setting (Fig. 1B and Fig. 1C). The effect depended monotonously on both  $E$  and  $\beta$  (single-run simulation examples in Fig. 1C-D, further detail in Fig. S2A-E).

Repeating simulations runs 10 times with 2000 particles each, for each scenario, provided a robust summary (Fig. 1E and Fig. S2F), suggesting that in obstacle-filled media the relationship between field strength and ion transfer (current) is sub-linear. It appears therefore that the obstacles decelerate ion movement to a disproportionately greater degree in stronger fields. Reassuringly, in these simulations the  $D_{app} / D_{free}$  ratios representing diffusion diffusion permeability  $\theta$  were, under  $E = 0$ , in good correspondence with the Maxwell's relationship for porous media (35)  $D_{app} = \frac{2\alpha D_{free}}{3-\alpha}$  where porosity  $\alpha = 1 - \beta$  (Fig. 1E, open circles). However, under  $E > 0$ , our data suggest that porous-medium electric resistance, or ion diffusion permeability, depends on the field strength, rather than on the medium properties alone, thus deviating from the Ohm's law.

### Electrodiffusion in radial 2D and 3D electric fields

Molecular diffusion inside narrow 2D clefts with a local current point-source is a common scenario in the brain neuropil where inter-cellular signal exchange occurs in an electrolyte medium between the opposing cell membranes populated with ion channels. Our next test was therefore to release diffusing particles in the 20 nm wide (characteristic interstitial width)

flat cleft, with an accelerating radial field (Fig. 2A-B). For simplicity, field strength  $E$  was maintained uniform: we have previously shown that in the 2D synaptic cleft, with a spatially uniform distribution of postsynaptic channels, the field is closer to uniform than to the classical  $r^{-1}$  decay for radial field with cylindrical symmetry ( $r$  is the distance from the centre). Furthermore, when the diffusion distance of interest is much smaller than the distance from the field source, uniform field provides canonical linear approximation. An additional reason for keeping uniform  $E$  was to try and separate the effects of field geometry and field strength on diffusion permeability. Other simulation parameters were similar to the 1D case shown above (Fig. 1). Again, the simulation outcome suggested that the electric fields, while accelerating overall diffusion escape of charged molecules compared to the zero-field case, reduced medium diffusion permeability  $\theta$  for ions, as reported by the decreased  $D_{app} / D_{free}$  ratios in stronger fields (Fig. 2C; Fig. S3).

Finally, we explored a similar scenario in three dimensions. For the sake of generality, we expanded the simulation arena to 10  $\mu\text{m}$  and increased the diameter of diffusion-hindering spheres to the range of 0.1-1  $\mu\text{m}$  (uniformly distributed; snapshot in Fig. 2D, Fig. S4A) and time step  $\Delta t = 0.1 \mu\text{s}$ . Similar to the cases considered above, here we found a clear, albeit less strong, reduction in the  $D_{app} / D_{free}$  ratios, hence diffusion permeability  $\theta$ , either with stronger electric fields or with greater values of  $\beta$  (Fig. 2E, Fig. S4B-F).

We note that in these simulations the actual dimensions are mainly for illustration purposes: the dependence between field strength and medium diffusion permeability remains unchanged when the arena geometry, diffusion coefficient, and electric field are scaled by the same time and space factor. Our data also suggest that the effect of field on medium diffusion permeability is progressively weaker under radial fields with higher dimensions, at least in the vicinity of the source, as modelled here (Fig. 3A), even when the field strength is kept the same throughout the space. As mentioned above, at large distances from the source one would expect the local field to be well approximated by the 1D case.

### **Geometric obstacles and classical electrodiffusion theory**

It was important to assess how our MC simulation results are related to the classical Nernst-Planck (NP) theory. First, for the sake of generality, we tested whether positioning the field

source near the diffusion source, or away from it produced the same time-averaged apparent diffusion coefficient in our settings. Control MC runs confirmed that this was the case: particles showed a characteristic wave-like scatter away from the field source, showing the convergence of  $D_{app}$  for varied distance between the field and the diffusion sources (Fig. 3B).

Next, we systematically compared the particle concentration profiles computed using MC simulations with those obtained using analytical solutions of the canonical NP equation (Equation 2) which could be written in the form:

$$\frac{1}{D} \frac{\partial C}{\partial t} = \nabla \cdot \left( \nabla C - \frac{e}{kT} C \mathbf{E} \right) \quad (3)$$

where  $e$  is elementary unit charge, and  $k$  is the Boltzmann constant. For several cases of  $\beta > 0$  and  $E$  values, we thus calculated an analytical solution of the NP equation at certain time point ( $t = 100 \mu\text{s}$ ), first for diffusivity  $D_{E=0}$  estimated by MC simulations under  $E = 0$ . This solution was compared with the analytical solution calculated for diffusivity  $D_{app}$  estimated from MC simulations under the corresponding  $E > 0$  value. These cases were also compared with the concentration profile obtained directly by MC simulations under the same conditions.

As expected, in all cases under  $E > 0$  the concentration profiles showed a characteristic wave that was spreading away from the diffusion source (Fig. 3C-F). Reassuringly, in a free medium ( $\beta = 0$ ), MC simulations provided an excellent match with the analytical NP solution for a given  $E$  (Fig. 3C and 3E). In contrast, in an obstacle-filled medium ( $\beta > 0$ ), the classical NP theory overestimated the effective diffusivity values, with the discrepancy increasing with stronger fields (Fig. 3D and 3F). In other words, the outcome of MC simulations could be satisfactorily described using the analytical NP theory, but with a diffusion coefficient corrected for the field-dependent transfer retardation.

### Physical testing of electrodiffusion in a porous medium

To test our theoretical prediction that the ion conductance of porous media is field-dependent, we designed and implemented a simple physical experiment. We measured electrolyte currents between the opposite sides (flat parallel walls serving as electrodes) of a narrow

rectangular chamber filled with microscopic glass spheres (Fig. 4A-B; Methods), a design somewhat similar to that explored previously (36). The space fraction  $\beta$  occupied by the spheres was evaluated by monitoring electrolyte displacement in the chamber upon sphere filling,  $\beta = 0.30 \pm 0.02$ . We used 10 ms square voltage pulses over a range of voltages that would generate inside the chamber electric fields compatible with those in the brain tissue (Fig. 4C; Materials and Methods). The three solutions tested were water, NaCl (153 mM), and standard artificial cerebrospinal fluid (ACSF, Materials and Methods).

As expected, these measurements showed monotonic, quasi-linear dependencies between voltage (electric field) and electrolyte current in either free-space or sphere-filled chambers (Fig. 5A; water provided control measurements). However, because physical properties of electrolytes could be affected by electric field, it was important to compare these measurements directly between free and obstacle-filled cases under the same field strength: the ratio between the corresponding current density values (porous-to-free) should represent  $\theta = D_{app} / D_{free}$ . We thus found that  $\theta$  decreased with greater strengths of the electric field, both for ACSF and NaCl solutions (Fig. 5B, data points). This dependence was similar to that obtained in MC simulations of 1D electrodiffusion for  $\beta$  values roughly between 0.3 and 0.4 (Fig. 5B, dotted lines), which was a remarkable correspondence given that the volume fraction occupied by glass spheres in these experiments was  $\beta \sim 0.3$ . The slight shift of theoretical curves towards higher values of  $\beta$  (Fig. 5B) was likely because simulated spheres were allowed to overlap thus leading to somewhat higher space tortuosity. It appeared therefore that the electrical resistance of tested electrolytes in a porous space depended on the external electric field, in good correspondence with our theoretical predictions.

### Theoretical insight

Given the unlimited variety of porous medium geometries, it would not seem feasible to generalise our findings as a fully-fledged electrodiffusion theory. However, we sought to explore the first principles, by considering geometric obstacles as barriers in the field potential profile that drives ion diffusion transfer. For one-dimensional diffusion (which is 3D diffusion in a long narrow cylinder), the mean-square displacement of a free Brownian particle increases linearly with time  $t$ ,  $\langle x^2 \rangle \sim t$ , plus an additional drift when electric field is present (Fig. 5C, *i-ii*; red lines illustrate potential profiles for stronger and weaker field).

When the diffusing particle encounters an obstacle or a trap, it takes additional time  $\tau$  to escape it, so that particle displacement over time  $t$  is reduced to  $\langle x^2 \rangle \sim t^{\alpha(\tau)}$  where  $0 < \alpha(\tau) < 1$ .

1. The obstacle-imposed additional dwell time  $\tau$  depends on the characteristic height of the potential barrier (or trap)  $H$  (Fig. 5C, *iii*). Generally, for diffusion under electric field (electrodifusion),  $H$  scales with field strength  $E$  (Fig. 5C, *iii*; red lines illustrate how the potential barrier scales with the field strength). It has long been established that 1D stochastic diffusion in field  $E$  can be described by the canonical Dynkin's operator

$$\Psi = \frac{qDFE}{RT} \frac{d}{dx} + D \frac{d^2}{dx^2} \quad (\text{p. 241 in (37)})$$

in which the first and second terms define electric drift and free diffusion, respectively;  $R$  is the gas constant,  $T$  is the temperature,  $F$  is the Faraday constant. When field  $E$  is directed against particle's escape over a certain barrier, the mean exit (dwell) time  $\tau$  is given by the boundary value problem  $-\Psi \tau = 1$  with the Dirichlet boundary condition. This leads to the steady-state equation (38):

$$D \left( \frac{\partial^2 \tau}{\partial x^2} + \frac{qFE}{RT} \frac{\partial \tau}{\partial x} \right) = -1 \quad (4)$$

with the boundary conditions

$$\tau(x=0) = 0, \quad \frac{\partial \tau}{\partial x}(x=H) = 0$$

where  $x$  in this case denotes the initial particle's coordinate (between 0 and  $H$ ). Its solution for  $\tau$  is

$$\tau(x) = \frac{e^{(-\kappa EH)} (1 - e^{\kappa Ex} + e^{\kappa EH} \kappa Ex)}{(\kappa E)^2 D} \quad (5)$$

where  $\kappa = RT/F$ . For  $x = H$  (displacement to the edge of the barrier  $H$ ), Eq. 5 becomes

$$\tau_-(H) = \frac{\kappa EH - 1 + e^{(-\kappa EH)}}{(\kappa E)^2 D} \quad (6)$$

Eq. 6 thus describes the average barrier-imposed dwell time  $\tau_-$  (Fig. 5C, *iii*). This time defines diffusion deceleration (time delay) when a particle faces an obstacle so that field  $E$  hinders its diffusion escape. In this case, particle displacement is reduced compared to free diffusion. On the same space-time scale, when the particle is behind the trap in the direction

of  $E$ , or otherwise if the field is reversed (to  $-E$ ), it gains an additional drift along  $E$ , because any stochastic movement in the opposite direction is prevented by the barrier (Fig. 5C, *iv*). This increase in drift, when compared to free-medium diffusion, translates into time gain:

$$\tau_+(H) = \frac{-\kappa EH - 1 + e^{(\kappa EH)}}{(\kappa E)^2 D} \quad (7)$$

Then, relative medium conductivity estimate  $\theta$  under field  $E$  could be estimated by the expression

$$\theta(H) = \theta_0 \frac{\tau_-(H)}{\tau_+(H)} = \theta_0 \frac{\kappa EH - 1 + e^{(-\kappa EH)}}{-\kappa EH - 1 + e^{(\kappa EH)}} \quad (8)$$

where  $\theta_0$  is the relative medium conductance (porous versus obstacle-free) under zero-field ( $E = 0$ ). In our experimental settings (Fig. 4), the  $\theta_0$  value is estimated between 0.4 and 0.5 (Fig. 5B), so that Eq. 8 has one free parameter  $H$ . It turns out that, with the  $H$  values set between 5 and 10  $\mu\text{m}$ , Eq. 8 provides a reasonably close prediction of the experimental dependence between relative conductivity  $\theta$  and field strength (Fig. 5D).

What could be the meaning of  $H$  values in our experimental test (Fig. 4)? Several studies suggest that the space tortuosity for a sphere-packed medium with  $\beta = 0.3-0.4$  ranges between 1.3-1.5 (39-41). This implies a 30-50% increase in the particle's diffusing path compared to an obstacle-free medium. With the characteristic sphere radius in our tests of  $\sim 15 \mu\text{m}$  (Fig. 4C), this increase corresponds to  $\sim 5-7 \mu\text{m}$  additional path per obstacle, which falls within the range of 'best-fit'  $H$  values of 5 and 10  $\mu\text{m}$ . Whether Eq. 8, and the meaning of  $H$ , hold in more general cases remains an open and intriguing question.

## DISCUSSION

The main finding of the present study is that diffusion permeability of porous (obstacle-filled) media for charged particles could depend on the macroscopic electric field. MC simulations predicted that the apparent diffusion coefficient, or electrical conductivity, in such media decreases with stronger electric fields which otherwise accelerate diffusion transfer. This

dependence is enhanced with increased geometric hindrance, or decreased porosity. Our data also suggest that the additional diffusion hindrance due to the electric field effect is weaker in radial compared to uniform field, even when the field strength remains the same throughout the space. The latter observation might help explain conclusions of an earlier study (42), in which geometric considerations suggested a longer diffusion path for '1D diffusion' compared to point-source diffusion in 2D or 3D: in fact, these conclusions should have referred to ion diffusion in a strong uniform (1D) field compared to radial fields. One could also consider a limiting case when the electric field drift dwarfs any stochastic Brownian effects: in that case, space dead-ends in the porous media (4, 43, 44) could entirely prevent particle transfer.

### **Modelling electrodiffusion**

The MC algorithms for diffusion and electrodiffusion employed here have previously been tested and validated systematically against experimental recordings, including sub-millisecond fast-exchange receptor probing in outside-out and nucleated (whole-cell) membrane patches (25, 26). In the present study, we compared the MC simulation outcome with the analytical solutions of the Nernst-Planck equation, in several key settings, and found good correspondence. Throughout our analyses, we assumed no interactions between diffusing particles and the spherical obstacles, such as any electrostatic or electroosmotic influence: we tried to focus on the case of small ions diffusing, on the microscopic scale, in the weak (fully-dissociated) electrolyte filled with macromolecules and other inert nanoscopic obstacles. This may not necessarily be the case when particles diffuse in sufficiently narrow clefts between charged surfaces, which may give rise to further interference with their transfer (20, 22). In this context, our MC algorithms enabled diffusing particles to navigate individual obstacles, roughly in correspondence with the distortions of electric field near the surface of dielectric (low permittivity) spheres. Whilst it would be important to have a more rigorous assessment of particle behaviour in the vicinity of obstacles, the particle concentration profiles generated by our MC simulations appeared in good agreement with the Nernst-Planck solutions incorporating the apparent diffusion coefficient.

We tested our theoretical predictions using a simple physical experiment in which the relationship between electric current and external field was measured in controlled conditions

involving glass sphere-filled electrolyte solutions. The electrolyte strength was sufficiently low (much below 0.2 M) to assume free ion mobility (full dissociation) without ion-ion interactions whereas the porosity value was high enough ( $\sim 0.7$ ) to ignore electrostatic interactions with the sphere walls. The shape and the material of obstacles can also affect interpretation of the results. In our tests, soda glass microbeads were selected for the several reasons. First, we aimed to match the geometry (if not size) of obstacles in our MC simulations. Second, solid glass material has high crush strength which makes it suitable for high-density packing. Third, soda glass helped to avoid polarisation effects in the spheres if compared with other materials like polystyrene or coated metals. Although the experiment did not replicate the dimensions of the MC simulation settings, we considered it suitable enough to address the underlying principle. In addition, our control MC simulations suggested that having either overlapping spheres (as we did throughout our tests) or non-overlapping spheres (in the experiment) had indistinguishably similar effects on the apparent diffusion coefficient, at least for  $\beta < 0.5$ .

### **Potential implications for electrophysiology**

Across the areas of biology (and other sciences), porous media come with highly variable geometries and electrodiffusion scenarios. This makes it difficult to suggest a generalised theory, although significant progress has been made in the description of ion flows in media consisting of tightly packed obstacles separated by narrow pores (such as porous rocks, sediments, ceramics, etc.) (20, 21). Recently, an elegant study has introduced a Kirchhoff-Nernst-Planck formalism, in order to model macroscopic electrodiffusion in the interstitial space surrounding nerve cells (22). On the nanoscale in the brain, a better understanding of electrodiffusion phenomena is beginning to emerge (23, 45), reflecting a present gap in our knowledge (2, 46). In this context, much less attention has been paid to the potential influence of electric fields on the conductive properties of obstacle-filled electrolytes in biological tissues. The potential importance of this issue stems from the clear dependence between extracellular ion current (both diffusive and resistive components) and the external field frequency in brain tissue (15, 17). Such non-ohmic properties of the brain extracellular medium can be related to the local structural inhomogeneities, so that the time scale of changes in the field strength and/or direction affects local ion flow differently, depending on

the size of local obstacles (16). This appears consistent, in principle, with our present conclusions that relate field strength (and  $\beta$ ) to medium diffusion permeability.

One potentially important consequence of having local non-ohmic properties of the brain tissue is the quantitative interpretation of electrocorticography of field-potential recordings. Such recordings reflect the strength, spatial distribution, and preferred orientation of local current sources and sinks inside the tissue volume conductor: estimating these parameters from the (multi-point) field-potential readout constitutes the classical inverse problem of brain electrophysiology (18). Introducing non-ohmic tissue properties that might arise from our present findings might therefore lead to somewhat differing estimates pertaining to the arrangement and strength of active current sources across the frequency spectrum (16, 18). This could in turn affect our understanding of electrical neural network activity based on the current-source reconstruction from electrophysiological recordings.

Here, we have attempted a first-principle theoretical treatment in which geometrical obstacles are considered potential barriers in the homogenous electric field. It appears that, under plausible assumptions, and within the tested range of experimental parameters, the theory provides a reasonable prediction of the dependence between electric field strength and relative reduction in conductivity observed experimentally. Clearly, further tests should answer the question how general these theoretical findings are.

**AUTHORS CONTRIBUTIONS**

L.P.S. designed and carried out Monte Carlo simulations and developed analytical theory; K.Z. designed and implemented physical tests; L.P.S., K.Z., and D.A.R. analysed the data; D.A.R. narrated the study, designed selected approaches, and wrote the manuscript which was contributed to by all authors.

**ACKNOWLEDGEMENTS**

This work was supported by the Wellcome Trust Principal Fellowship Award (212251\_Z\_18\_Z), ERC Advanced Grant (323113) and European Commission NEUROTWIN grant (857562), to D.A.R. Optimization and parallelization of computing algorithms were implemented by AMC Bridge LLC (Waltham, MA).

## REFERENCES

1. Sykova, E., and C. Nicholson. 2008. Diffusion in brain extracellular space. *Physiol. Rev.* 88(4):1277-1340.
2. Savtchenko, L. P., M. M. Poo, and D. A. Rusakov. 2017. Electrodiffusion phenomena in neuroscience: a neglected companion. *Nat Rev Neurosci* 18(10):598-612.
3. Nicholson, C., and L. Tao. 1993. Hindered Diffusion of High-Molecular-Weight Compounds in Brain Extracellular Microenvironment Measured with Integrative Optical Imaging. *Biophys J* 65(6):2277-2290.
4. Hrabe, J., S. Hrabetova, and K. Segeth. 2004. A model of effective diffusion and tortuosity in the extracellular space of the brain. *Biophys J* 87(3):1606-1617.
5. Zheng, K., A. Scimemi, and D. A. Rusakov. 2008. Receptor actions of synaptically released glutamate: the role of transporters on the scale from nanometers to microns. *Biophys J* 95(10):4584-4596.
6. Zhang, H., and A. S. Verkman. 2010. Microfiber-optic measurement of extracellular space volume in brain and tumor slices based on fluorescent dye partitioning. *Biophys J* 99(4):1284-1291.
7. Arizono, M., V. Inavalli, A. Panatier, T. Pfeiffer, J. Angibaud, F. Levet, M. J. T. Ter Veer, J. Stobart, L. Bellocchio, K. Mikoshiba, G. Marsicano, B. Weber, S. H. R. Oliet, and U. V. Nagerl. 2020. Structural basis of astrocytic Ca(2+) signals at tripartite synapses. *Nat Commun* 11(1):1906.
8. Tonnesen, J., V. V. G. K. Inavalli, and U. V. Nagerl. 2018. Super-resolution imaging of the extracellular space in living brain tissue. *Cell* 172:1108-1121.
9. Zheng, K. Y., T. P. Jensen, L. P. Savtchenko, J. A. Levitt, K. Suhling, and D. A. Rusakov. 2017. Nanoscale diffusion in the synaptic cleft and beyond measured with time-resolved fluorescence anisotropy imaging. *Scientific Reports* 7:42022.
10. Cai, J. C., W. Wei, X. Y. Hu, and D. A. Wood. 2017. Electrical conductivity models in saturated porous media: A review. *Earth-Sci Rev* 171:419-433.
11. Bussian, A. E. 1983. Electrical Conductance in a Porous-Medium. *Geophysics* 48(9):1258-1268.
12. Bedard, C., and A. Destexhe. 2009. Macroscopic Models of Local Field Potentials and the Apparent 1/f Noise in Brain Activity. *Biophys J* 96(7):2589-2603.
13. Li, G. L., and B. M. M. Fu. 2011. An Electrodiffusion Model for the Blood-Brain Barrier Permeability to Charged Molecules. *Journal of Biomechanical Engineering-Transactions of the Asme* 133(2).
14. Bedard, C., and A. Destexhe. 2011. Generalized theory for current-source-density analysis in brain tissue. *Physical Review E* 84(4).
15. Gomes, J. M., C. Bedard, S. Valtcheva, M. Nelson, V. Khokhlova, P. Pouget, L. Venance, T. Bal, and A. Destexhe. 2016. Intracellular Impedance Measurements Reveal Non-ohmic Properties of the Extracellular Medium around Neurons. *Biophys J* 110(1):234-246.

16. Nelson, M. J., C. Bosch, L. Venance, and P. Pouget. 2013. Microscale Inhomogeneity of Brain Tissue Distorts Electrical Signal Propagation. *J. Neurosci.* 33(7):2821-2827.
17. Logothetis, N. K., C. Kayser, and A. Oeltermann. 2007. In vivo measurement of cortical impedance spectrum in monkeys: Implications for signal propagation. *Neuron* 55(5):809-823.
18. Buzsaki, G., C. A. Anastassiou, and C. Koch. 2012. The origin of extracellular fields and currents--EEG, ECoG, LFP and spikes. *Nat Rev Neurosci* 13(6):407-420.
19. Zhang, Y. Y., G. S. Wang, K. F. Wang, Y. Wang, and X. L. Dong. 2008. The model of electric field dependent dielectric properties for porous ceramics. *J Appl Phys* 103(11).
20. Di Fraia, S., N. Massarotti, and P. Nithiarasu. 2018. Modelling electro-osmotic flow in porous media: a review. *Int J Numer Method H* 28(2):472-497.
21. Szyszkiewicz, K., J. J. Jasielec, M. Danielewski, A. Lewenstam, and R. Filipek. 2017. Modeling of Electrodifusion Processes from Nano to Macro Scale. *J Electrochem Soc* 164(11):E3559-E3568.
22. Solbra, A., A. W. Bergersen, J. van den Brink, A. Malthe-Sorensen, G. T. Einevoll, and G. Haines. 2018. A Kirchhoff-Nernst-Planck framework for modeling large scale extracellular electrodiffusion surrounding morphologically detailed neurons. *PLoS Computational Biology* 14(10).
23. Holcman, D., N. Hoze, and Z. Schuss. 2011. Narrow escape through a funnel and effective diffusion on a crowded membrane. *Physical Review E* 84(2).
24. Biess, A., E. Korkotian, and D. Holcman. 2011. Barriers to diffusion in dendrites and estimation of calcium spread following synaptic inputs. *PLoS Comput Biol* 7(10):e1002182.
25. Savtchenko, L. P., S. Sylantsev, and D. A. Rusakov. 2013. Central synapses release a resource-efficient amount of glutamate. *Nature Neurosci.* 16(1):10-U163.
26. Sylantsev, S., L. P. Savtchenko, Y. Ermolyuk, P. Michaluk, and D. A. Rusakov. 2013. Spike-Driven Glutamate Electrodiffusion Triggers Synaptic Potentiation via a Homer-Dependent mGluR-NMDAR Link. *Neuron* 77(3):528-541.
27. Savtchenko, L. P., S. N. Antropov, and S. M. Korogod. 2000. Effect of voltage drop within the synaptic cleft on the current and voltage generated at a single synapse. *Biophys J* 78(3):1119-1125.
28. Savtchenko, L. P., and D. A. Rusakov. 2007. The optimal height of the synaptic cleft. *Proc Natl Acad Sci U S A* 104(6):1823-1828.
29. Conway, J. H., and N. J. A. Sloane. 1995. What Are All the Best Sphere Packings in Low Dimensions. *Discrete Comput Geom* 13(3-4):383-403.
30. Kimberly, E. E., editor. 1939. *Electrical Engineering*. The Haddon Craftsmen Inc, Scranton, Pennsylvania.
31. Levitt, D. G. 1985. Strong Electrolyte Continuum Theory Solution for Equilibrium Profiles, Diffusion Limitation, and Conductance in Charged Ion Channels. *Biophys J* 48(1):19-31.
32. Holcman, D., and Z. Schuss. 2017. 100 years after Smoluchowski: stochastic processes in cell biology. *J Phys a-Math Theor* 50(9).

33. Hrabetova, S. 2005. Extracellular diffusion is fast and isotropic in the stratum radiatum of hippocampal CA1 region in rat brain slices. *Hippocampus* 15(4):441-450.
34. Tao, L., and C. Nicholson. 2004. Maximum geometrical hindrance to diffusion in brain extracellular space surrounding uniformly spaced convex cells. *J Theor Biol* 229(1):59-68.
35. Weissberg, H. L. 1963. Effective Diffusion Coefficient in Porous Media. *J Appl Phys* 34(9):2636-&.
36. Eberhardt, W., D. Woidich, and A. Reichenbach. 1990. Determination of the extracellular tortuosity in nuclear layers of the central nervous system by resistance measurements on a geometrical model. *J Hirnforsch* 31(1):1-11.
37. Dynkin, E. B. 1965. Markov processes. vol. Bände 121. Die Grundlehren der Mathematischen Wissenschaften. Academic Press, New York, p. 133.
38. Pavliotis, G. A. 2014. Stochastic Processes and Applications Diffusion Processes, the Fokker-Planck and Langevin Equations Preface. *Texts Appl Math* 60:Vii-+.
39. Ahmadi, M. M., S. Mohammadi, and A. N. Hayati. 2011. Analytical derivation of tortuosity and permeability of monosized spheres: A volume averaging approach. *Physical Review E* 83(2).
40. Boutin, C., and C. Geindreau. 2010. Periodic homogenization and consistent estimates of transport parameters through sphere and polyhedron packings in the whole porosity range. *Physical Review E* 82(3).
41. Pisani, L. 2011. Simple Expression for the Tortuosity of Porous Media. *Transport in Porous Media* 88(2):193-203.
42. Rusakov, D. A., and D. M. Kullmann. 1998. Geometric and viscous components of the tortuosity of the extracellular space in the brain. *Proc Natl Acad Sci U S A* 95(15):8975-8980.
43. Hrabetova, S., J. Hrabe, and C. Nicholson. 2003. Dead-space microdomains hinder extracellular diffusion in rat neocortex during ischemia. *J. Neurosci.* 23(23):8351-8359.
44. Binder, D. K., M. C. Papadopoulos, P. M. Haggie, and A. S. Verkman. 2004. In vivo measurement of brain extracellular space diffusion by cortical surface photobleaching. *J Neurosci* 24(37):8049-8056.
45. Cartailier, J., and D. Holcman. 2018. Electrical transient laws in neuronal microdomains based on electro-diffusion. *Phys Chem Chem Phys* 20(32):21062-21067.
46. Holcman, D., and R. Yuste. 2015. The new nanophysiology: regulation of ionic flow in neuronal subcompartments. *Nat Rev Neurosci* 16(11):685-692.

**FIGURE LEGEND****Figure 1. Ion diffusion permeability of obstacle-filled media in uniform electric field depends on field strength.**

(A) MC simulations: snapshot of the scatter of diffusing particles (blue dots) in a 0.1  $\mu\text{m}$  wide - 10  $\mu\text{m}$  long cylinder (fragment; two different scales as shown; actual simulation data rendered by OriginPro), at 0.1 ms post-release from the centroid (dotted line), with  $\beta = 0.2$  volume fraction occupied by obstacles (yellow spheres, 3-33 nm diameter), and electric field strength  $E = 0$ ; blue arrows, field direction.

(B) Example of a MC simulation run: time course of apparent diffusivity  $D_{app}$  (along the cylinder as in A) for different values of  $\beta$  as indicated.

(C) Example of a MC simulation run: time course of diffusion permeability  $\theta = D_{app} / D_{free}$ , under electric field  $E = E_0$  ( $10^4$  V/m), over the range of  $\beta$  values as shown; see Materials and Methods for model parameters.

(D) Example of a MC simulation run: time course of  $\theta$  for a medium with for  $\beta = 0.5$ , over the range of  $E$  as indicated.

(E) Statistical summary of simulation experiments depicted in B-D (additional examples of individual MC runs are shown in Fig. S2); dots  $\pm$  error bars, diffusion permeability  $\theta = D_{app} / D_{free}$  (mean  $\pm$  s.e.m.) values for  $n = 10$  runs completed for each set of  $\beta$  and  $E$  values, as indicated; the overall effect of either factor  $E$  (four levels) or  $\beta$  (four levels) on  $\theta$  is at  $p < 0.001$ , two-way ANOVA ( $F_E = 79.0$ ,  $F_\beta = 1366$ ).

**Figure 2. Ion diffusion permeability of obstacle-filled media in radial electric fields..**

(A) Simulation example: a scatter of diffusing particles (blue dots) in a 20 nm flat cleft extending 6  $\mu\text{m}$  wide (fragment; two different scales as shown; actual simulation data rendered by OriginPro); snapshot at 0.1 ms post-release at the central point (dotted line), with  $\beta = 0.2$  and  $E = 0$ ; blue arrows, radial field.

(B) Snapshots of single-particle trajectories at three time points, as indicated, with  $\beta = 0$  (red) and  $\beta = 0.2$  (black), under no field ( $E = 0$ ); blue dot, diffusion starting point.

(C) Statistical summary of simulations in A-B (examples of individual MC runs are shown in Fig. S3); dots, diffusion permeability  $\theta = D_{app} / D_{free}$  (mean  $\pm$  s.e.m.) values for  $n = 10$  runs completed for each set of  $\beta$  and  $E$  values, as indicated; the overall effect of either factor  $E$  (four levels) or  $\beta$  (four levels) on  $\theta$  is at  $p < 0.001$ , two-way ANOVA ( $F_E = 45.3$ ,  $F_\beta = 906$ ).

(D) Simulation example: a scatter of diffusing particles (blue dots) in a three-dimensional space (fragment; actual simulation data rendered by OriginPro); snapshot at 0.1 ms post-release at the central point (dotted line), with  $\beta = 0.2$  of space occupied by spherical obstacles

(yellow spheres), electric field strength  $E = 0$ ; radial electric field is centred at the co-ordinate origin.

(E) Statistical summary of simulation experiments depicted in C (examples of individual MC runs are shown in Fig. S3); the overall effect of either factor  $E$  (four levels) or  $\beta$  (four levels) on  $\theta$  is at  $p < 0.001$ , two-way ANOVA ( $F_E = 24.4$ ,  $F_\beta = 31.3$ ); other notation as in C.

**Figure 3. Classical electrodiffusion theory may overestimate apparent diffusivity when applied to a porous medium.**

(A) A summary of MC simulations (as in Figs. 1-2) showing the dependence between field strength and diffusion permeability  $\theta = D_{app} / D_{free}$  (normalised to the value at  $E = 0$ ), for two  $\beta$  values, in 1D uniform, and 2D and 3D radial electric fields, as indicated. The strongest dependence corresponds to 1D field at the higher  $\beta$ .

(B) Image panel: illustration of a MC test in which diffusing particles are released either at the field source (open circle, blue arrow, blue dots) or at a distance of 200 nm from it (red arrow, red dots), under  $E = E_0$  ( $10^4$  V/m); a snapshot 100  $\mu$ s post-release. Graph: tests showing the time course of  $D_{app} / D_{free}$  values for particle cohorts released at different distances from the field source, as indicated, in condition as above.

(C) Black line, analytical solution of the NP equation showing a particle concentration profile (normalised to maximum) against distance to the diffusion source for 2D radial field with no obstacles ( $\beta = 0$ ,  $D = D_{free}$ ), under  $E = E_0$ , at time point  $t = 0.1$  ms; red, outcome of MC simulations in similar conditions.

(D) Similar to C, but with  $\beta = 0.5$ ; blue, analytical solution of the NP equation in which apparent diffusivity  $D_{E=0}$  is derived by MC simulations for  $E = 0$  ( $\beta = 0.5$ ); black, a similar solution but with  $D_{app}$  calculated from MC simulations incorporating electric field  $E = E_0$  (as in Fig. 2C graph, for  $E = 1 \times E_0$ ,  $\beta = 0.5$ ); red, outcome of MC simulations, as indicated.

(E) Similar to C, but for 3D radial field with  $\beta = 0.2$  and  $E = 5E_0$ , as indicated. Other notations are as in C.

(F) Similar to D, but for 3D radial field with  $\beta = 0.2$  and  $E = 5E_0$ . Other notations as in D; blue, analytical solution of the NP equation in which  $D_{E=0}$  is derived by MC simulations for  $E = 0$  ( $\beta = 0.2$ ); black, a similar solution but with  $D_{app}$  derived by MC simulations under  $E = 5E_0$  (as in Fig. 2E data point at  $E = 1 \times 5E_0$ ,  $\beta = 0.2$ ).

**Figure 4. Experimental testing of obstacle-filled medium conductivity under varied electric fields.**

(A) Experiment schematic. The test solution, with or without glass beads, is placed in a cuvette equipped with flat side electrodes (Methods). Controlled application of  $\Delta V$  voltage steps to the electrodes induces electric current measured digitally, as depicted.

**(B)** Electrolyte solution (NaCl) filled with densely packed microscopic glass beads, shown in transmitted light (800 nm) at the top layer (left; scale bar 50  $\mu\text{m}$ ), and as fluorescent image (right; solution containing Alexa Fluor 488, two-photon excitation 800 nm; scale bar 20  $\mu\text{m}$ ).

**(C)** Time course of voltage pulse application (an example, top), and the current response in a free-medium (middle) and sphere-filled NaCl solution (bottom). Grey shade, sampled response area (first 3 ms after the pulse artefact).

**Figure 5. Electric conductivity of porous tissue decreases with stronger electric fields.**

**(A)** Recorded current density plotted against electric field in ACSF and NaCl solutions, with and without densely packed microscopic glass beads (as in Fig. 4), as indicated; control recordings with deionised water shown.

**(B)** Relative porous-medium conductivity (ratio between porous- and free-medium conductivity values) for ACSF and NaCl electrolytes, plotted against electric field. Dotted lines, theoretical dependencies calculated for ions diffusing in 1D uniform electric field (as in Fig. 1), for  $\beta = 0.4$  and  $\beta = 0.3$  (experimental value in Fig. 4 tests), as indicated.

**(C)** Schematic illustrating (not to scale) a theoretical approach (Equations 4-8); blue shade, probability density for particle occurrence (dot, starting point) under no electric field (*i*), under uniform field  $E$  (*ii*; dotted arrow, average drift), facing the barrier of radius  $H$  (*iii*;  $\tau_-$ , maximum dwell time 'lost' to navigate the barrier), and behind the barrier (*iv*; green dotted arrow, no-obstacle particle drift, as in *ii*; black arrow, average drift increased because of the 'gained' time  $\tau_+$ ); red lines illustrate profiles of field potential  $V(x)$  in 1D space, for weaker ( $E_1$ ) and stronger ( $E_2$ ) fields, with orange dots representing particles facing (*iii*) or past (*iv*) the potential barrier.

**(D)** Experimental data as in B, but with the theoretical dependencies (dashed and dotted-dashed lines) calculated from the analytical solution (Eq. 8), for several values of  $H$  and  $\theta_0$ , as indicated.

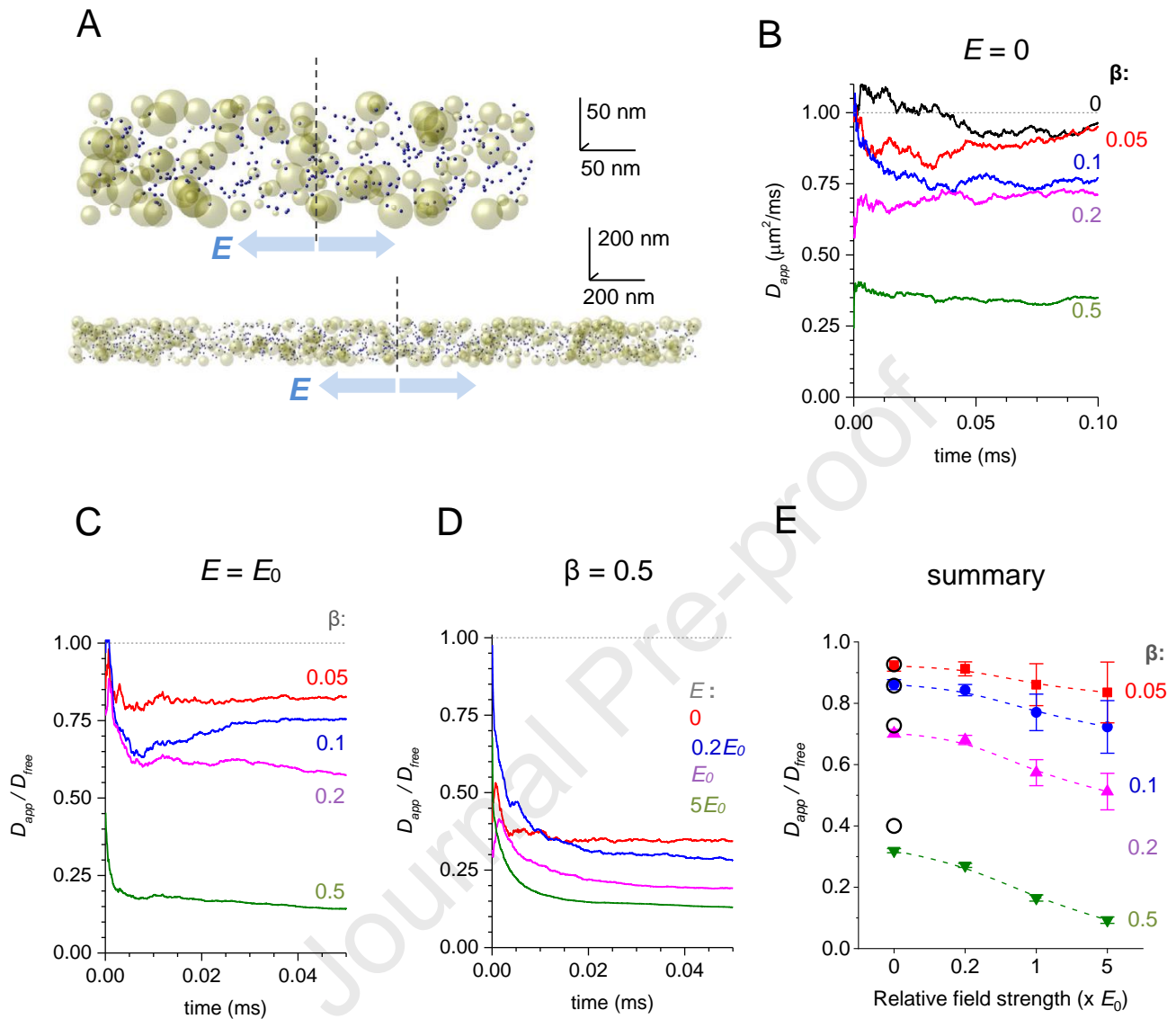


Figure 1

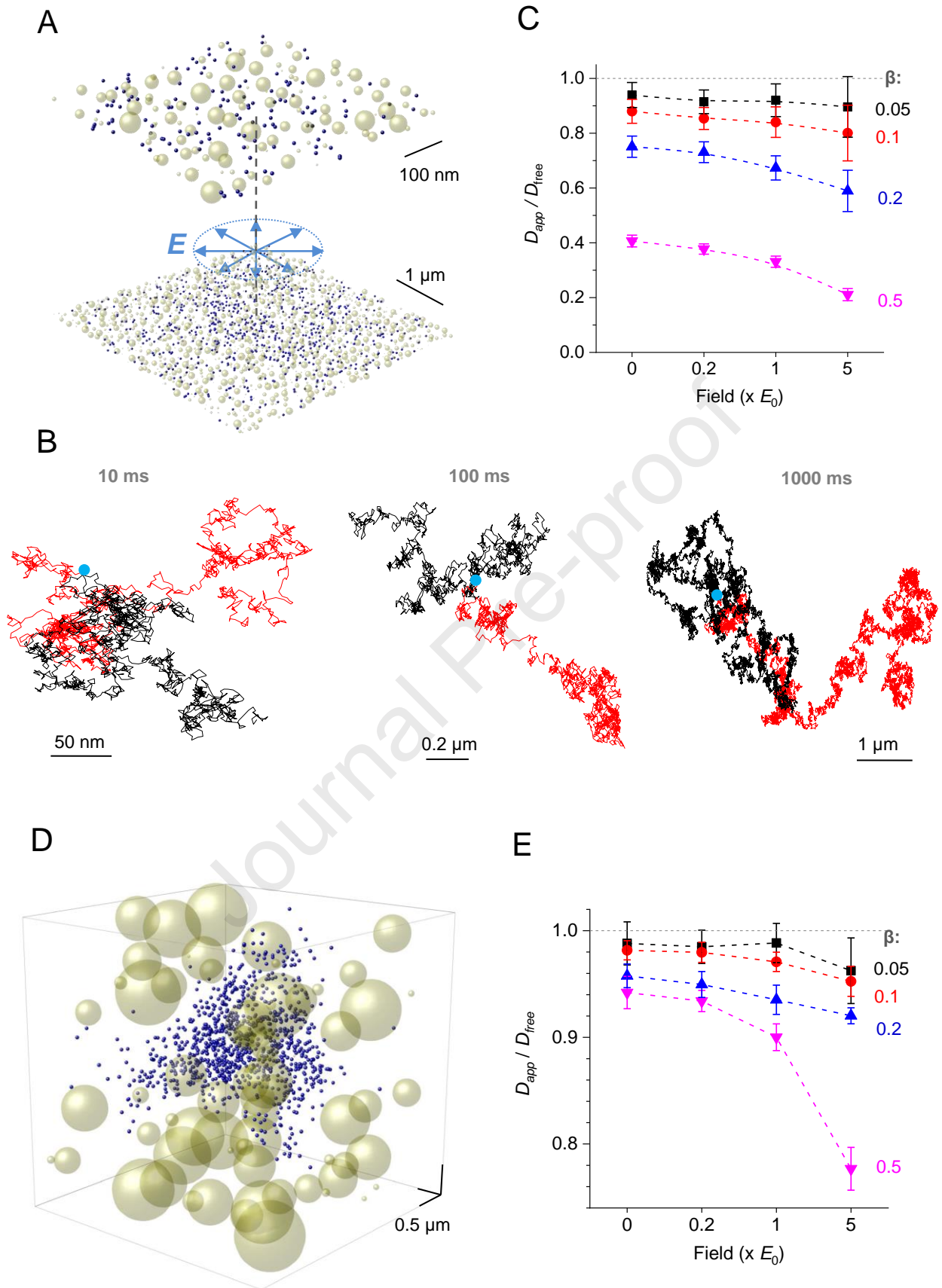


Figure 2

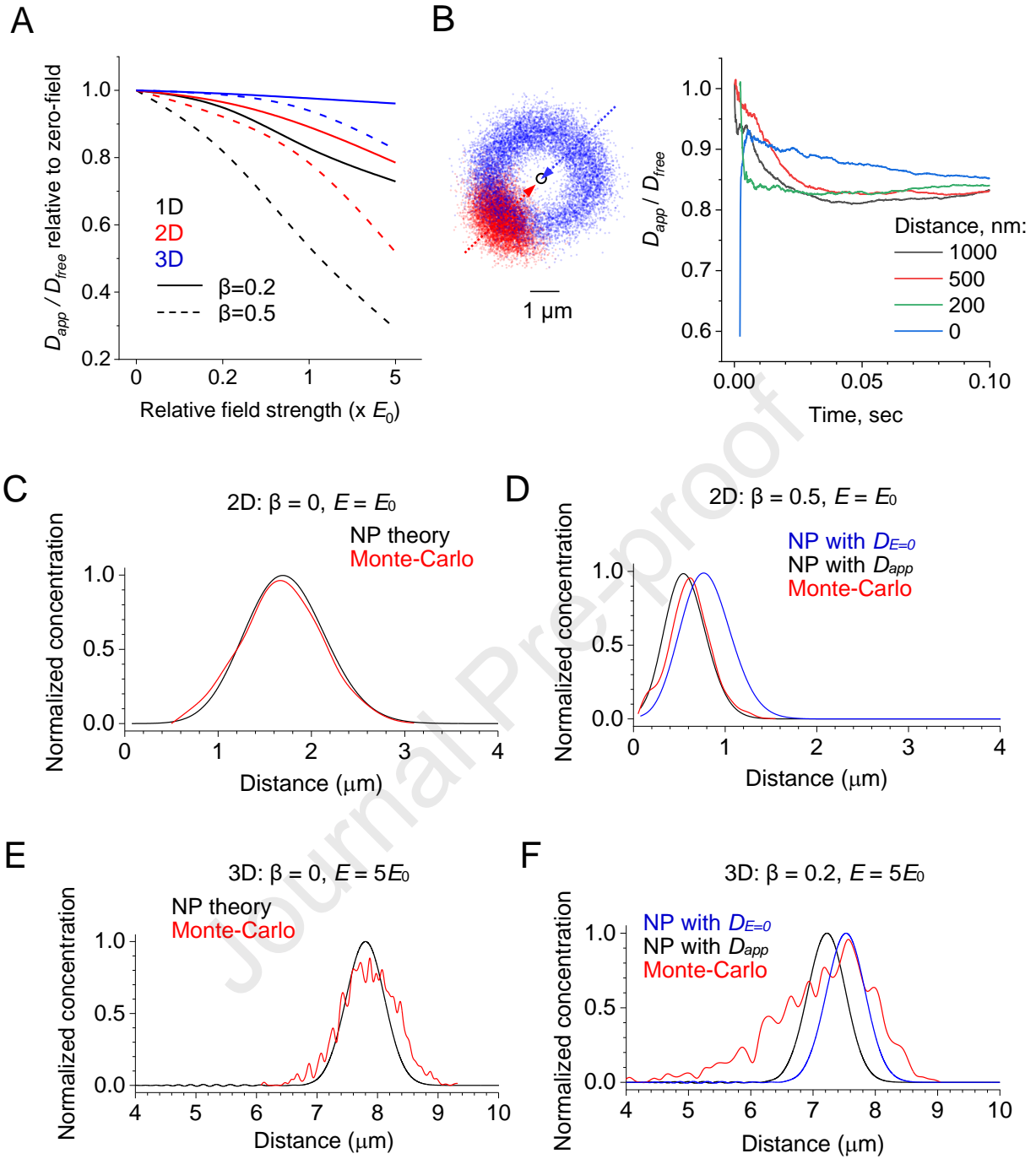


Figure 3

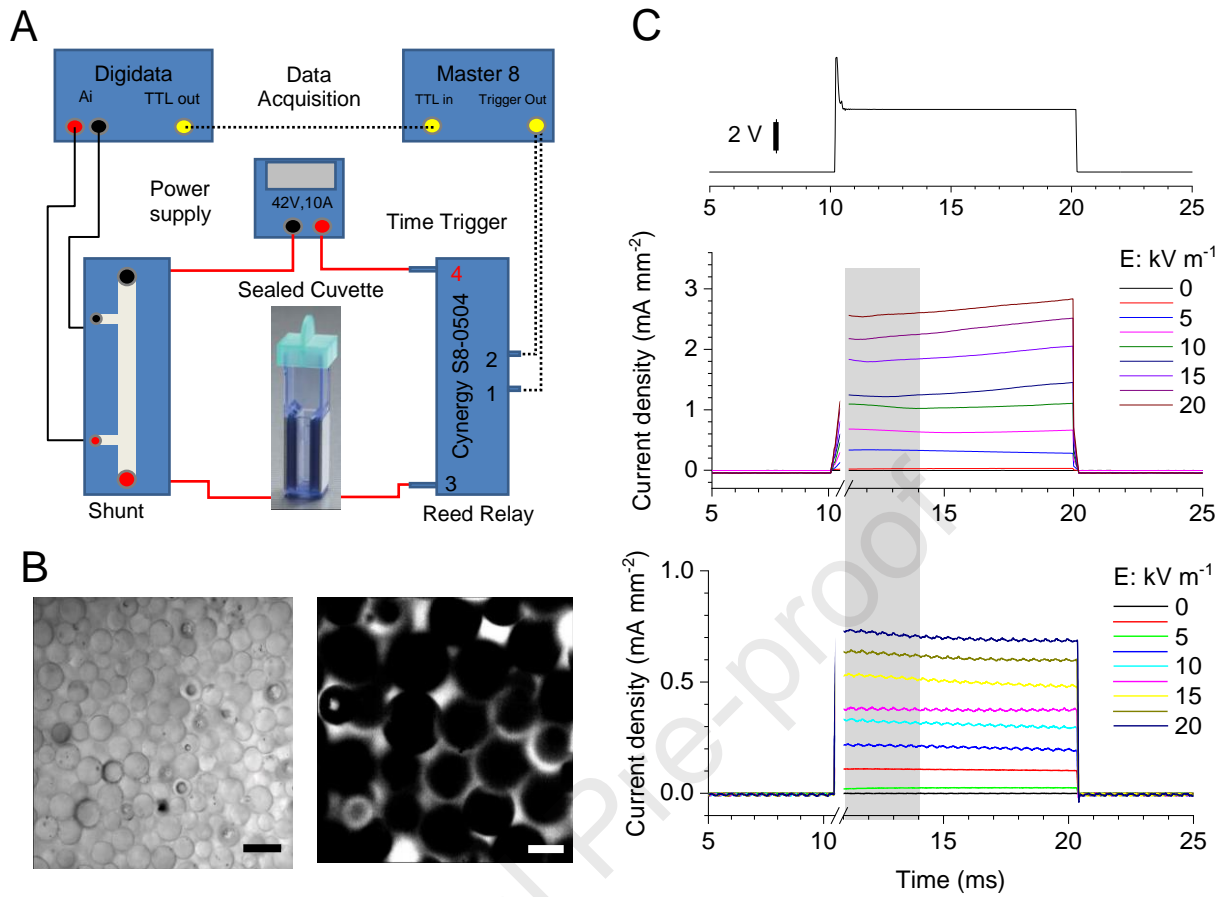


Figure 4

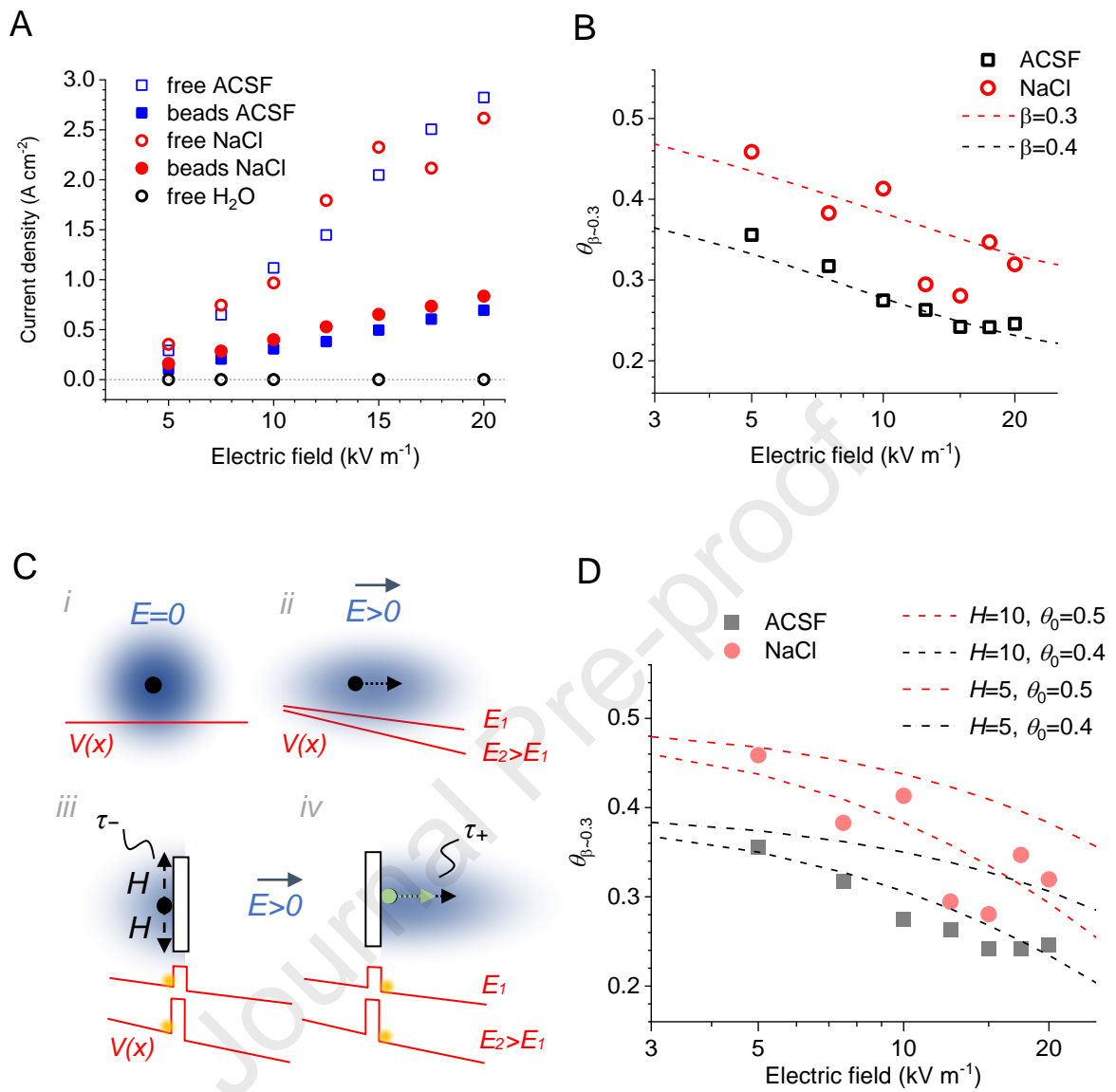


Figure 5